Supporting Information

Anti-Perovskite Carbides Ca$_6$CSe$_4$ and Sr$_6$CSe$_4$ for Photovoltaics with Similar Optoelectronic Properties to MAPbI$_3$

Wen-hui Guo,[a] Hong-xia Zhong,*[b] Juan Du,[a] Yao-hui Zhu,[c] Shi-ming Liu,[a]

Yong He,[a] Chong Tian,[a] Min Zhang,[d] Xinqiang Wang[a] and Jun-jie Shi*[a]

[a]*State Key Laboratory for Artificial Microstructures and Mesoscopic Physics, School of Physics, Peking University Yangtze Delta Institute of Optoelectronics, Peking University, Beijing 100871, China.*

[b]*School of Mathematics and Physics, China University of Geosciences, Wuhan 430074, China*

[c]*Physics Department, Beijing Technology and Business University, Beijing 100048, China*

[d]*Inner Mongolia Key Laboratory for Physics and Chemistry of Functional Materials, College of Physics and Electronic Information, Inner Mongolia Normal University, Hohhot 010022, China*

Corresponding authors: E-mail: zhonghongxia@cug.edu.cn, jjshi@pku.edu.cn

1. Calculation methods

1.1 DFT calculations

The highly efficient Vienna Ab-initio Simulation Package (VASP) based on the density functional theory (DFT) is employed in the first-principles calculations of the current anti-perovskite M_6CCh_4 (M=Ca, Sr, Ba; Ch=S, Se, Te) [1]. The electronic exchange-correlation (XC) functional is treated based on the generalized gradient approximation (GGA) of Perdew-Burke-Ernzerhof (PBE) [2]. The ion-electron interactions are described by the projector augmented wave (PAW) method [3, 4]. The cutoff energy for the plane-wave basis is set to 500 eV. An $11\times11\times11$ ($13\times13\times13$) Monkhorst-Pack grid is chosen for structure optimization (self-consistent calculation) in the Brillouin zone of the primitive unit.

1.2. Modified Becke-Johnson (mBJ) potential

Considering that GGA-PBE approach always underestimates the bandgap, in order to obtain the realistic bandgap value, the computationally cheap modified Becke-Johnson (mBJ) potential [5] was employed. The mBJ potential $v_{x,\sigma}^{mBJ}$ reads

$$v_{x,\sigma}^{mBJ}(r) = cv_{x,\sigma}^{BR}(r) + (3c-2)\frac{1}{\pi}\sqrt{\frac{5}{12}}\sqrt{\frac{2t_\sigma(r)}{\rho_\sigma(r)}},$$

where $\rho_\sigma(r)$ is the electron density, which is defined as

$$\rho_\sigma(r) = \sum_{i=1}^{N_\sigma}|\psi_{i,\sigma}|^2.$$

The kinetic-energy density $t_\sigma(r)$ can be calculated by

$$t_\sigma(r) = (1/2)\sum_{i=1}^{N_\sigma}\psi_{i,\sigma}^*\nabla\psi_{i,\sigma},$$

here, $\psi_{i,\sigma}$ is the one-electron wave functions.

The Becke-Roussel (BR) potential $v_{x,\sigma}^{BR}(r)$ was proposed to model the Coulomb potential created by the exchange hole [6].

$$v_{x,\sigma}^{BR}(r) = -\frac{1}{b_\sigma(r)}\left(1 - e^{-x_\sigma(r)} - \frac{1}{2}x_\sigma(r)e^{-x_\sigma(r)}\right),$$

here, $x_\sigma(r)$ is determined from a nonlinear equation involving ρ_σ, $\nabla\rho_\sigma$, $\nabla^2\rho_\sigma$, and t_σ, and then $b_\sigma(r)$ is calculated by

$$b_\sigma(r) = \left[x_\sigma^3(r)e^{-x_\sigma(r)}/(8\pi\rho_\sigma(r))\right]^{1/3},$$

$$c = \alpha + \beta\left(\frac{1}{V_{cell}}\int_{cell}\frac{|\nabla\rho(r')|}{\rho(r')}d^3r'\right)^{1/2},$$

here, V_{cell} is the unit cell volume. The parameters α and β can be modified to match with the accurate energy gap value.

1.3. Carrier mobility

According to Feynman et al. [7, 8], the carrier mobility μ can be obtained using the following formula [9, 10]

$$\mu = \frac{3e}{2\sqrt{\pi}c\omega_{LO}m^*\alpha} \frac{\sinh(\beta/2)}{\beta^{5/2}} \frac{\omega^3}{v^3} \frac{1}{K},$$

where e is the electron charge and c is the speed of light in the vacuum.

The effective mass m^* can be approximately defined by a quadratic relationship of the energy dispersion $m^* = \hbar^2[\partial^2 E(k)/\partial k^2]^{-1}$ at the bottom of the conduction band (top of the valence band). ω_{LO} is the average LO phonon frequency, which can be obtained by solving the following equation

$$\frac{W^2}{\omega_{LO}}\coth\left(\frac{hc\omega_{LO}}{2k_BT}\right) = \sum_{i=1}^{n}\frac{W_i^2}{\omega_{LO,i}}\left(\frac{hc\omega_{LO,i}}{2k_BT}\right),$$

here, h is the Planck constant, k_B is the Boltzmann constant, and T is the temperature. $W^2 = \sum_{i=1}^{n}W_i^2$, W_i is the oscillator strength of the i-th LO phonon branch, in accordance with Hellwarth and Biaggio, W_i can be calculated by

$$W_i^2 = \frac{1}{\varepsilon_\infty}\left(\omega_{LO,i}^2 - \omega_{TO,i}^2\right).$$

The parameter $\alpha = \frac{1}{\varepsilon^*}\sqrt{\frac{R_y}{ch\omega_{LO}}}\sqrt{m^*}$ is the Fröhlich electron-phonon coupling constant, here, R_y is the Rydberg energy, and $\frac{1}{\varepsilon^*}$ is the ionic screening parameter, which can be obtained by $\frac{1}{\varepsilon^*} = \frac{1}{\varepsilon_\infty} - \frac{1}{\varepsilon_0}$. Here, ε_∞ (ε_0) is the high-frequency (static) dielectric constant. The calculated dielectric functions of Ca$_6$CSe$_4$ and Sr$_6$CSe$_4$ are exhibited in Figure S11. β can be calculated by $\beta = hc\omega_{LO}/k_BT$. Both ω and v could be found by minimizing the free polaron energy F [11]:

$$F = -(A + B + C),$$

$$A = \frac{3}{\beta}\left[\ln\left(\frac{v}{\omega}\right) - \frac{\ln(2\pi\beta)}{2} - \ln\left(\frac{\sinh(v\beta/2)}{\sinh(\omega\beta/2)}\right)\right],$$

$$B = \frac{\alpha v}{\sqrt{\pi}[\exp(\beta)-1]}\int_0^{\beta/2}\frac{\exp(\beta-x)+\exp(x)}{\sqrt{\omega^2 x(1-x/\beta)+Y(x)(v^2-\omega^2)/v}}dx,$$

$$Y(x) = \frac{1}{1-\exp(-v\beta)}\{1 + \exp(-v\beta) - \exp(-vx) - \exp(v[x-\beta])\},$$

$$C = \frac{3(v^2-\omega^2)}{4v}\left[\coth\left(\frac{v\beta}{2}\right) - \frac{2}{v\beta}\right].$$

The parameter K is a function of β and the temperature-dependent variational parameters ω and v [9, 10, 12] shown in the following formula:

$$K(a,b) = \int_0^\infty \frac{\cos(u)}{[u^2+a^2-b\cos(vu)]^{3/2}}du,$$

$$a^2 = \left(\frac{\beta}{2}\right)^2 + R\beta\coth\left(\frac{\beta v}{2}\right),$$

$$b = \frac{R\beta}{\sinh(\beta v/2)},$$

$$R = \frac{v^2-\omega^2}{\omega^2 v}.$$

1.4. Optical absorption

To investigate the optical properties, we calculate the frequency-dependent dielectric matrix in the long-wavelength limit ($q \to 0$) using the sum over states approach [13]. In this case, the imaginary part of the dielectric function can be calculated by

$$\varepsilon_{\alpha\beta}^{(2)}(\omega) = \frac{4\pi^2 e^2}{\Omega} \lim_{q \to 0} \frac{1}{q^2} \sum_{c,v,k} 2\omega_k \delta(\varepsilon_{ck} - \varepsilon_{vk} - \omega) \times \langle u_{ck+\hat{e}_\alpha q} | u_{vk} \rangle \langle u_{vk+\hat{e}_\beta q} | u_{vk} \rangle^*,$$

where c and v represent the unoccupied and occupied bands, q is the wave number of the incident electromagnetic wave, Ω is the volume of the structure cell, u_{ck} (u_{vk}) is the periodic part of the orbitals at the k-point, and $\hat{e}_\alpha$ $(\hat{e}_\beta)$ represents the unit vector along the α (β) direction.

By using the Kramers-Kronig relationship [14], the real part of the dielectric function can be obtained by the following expression

$$\varepsilon_{\alpha\beta}^{(1)}(\omega) = 1 + \frac{2}{\pi} P \int_0^\infty \frac{\varepsilon_{\alpha\beta}^{(2)}(\omega')\omega'}{\omega'^2 - \omega^2 + i\eta} d\omega'.$$

Then the interband optical absorption coefficient $\alpha(\omega)$ can be calculated by the formula [15]

$$\alpha(\omega) = \sqrt{2}\omega \left[\sqrt{\varepsilon^{(1)}(\omega)^2 + \varepsilon^{(2)}(\omega)^2} - \varepsilon^{(1)}(\omega) \right]^{1/2}.$$

1.5. Melting point

The melting point T_0 (in K) is estimated by the empirical relation of $T_0 = 607 + 9.3B$ [16], where B (in GPa) is the bulk modulus. The bulk modulus can be obtained from corresponding elastic constants using Voigt-Reuss-Hill averaging [17-19] by using the VASPKIT code [20].

1.6. Exciton binding energy

The exciton binding energy E_b can be estimated by the Wannier model [21] of $E_b = R_y \frac{\mu^*}{\varepsilon_\infty^2}$, where R_y=13.56 eV is the atomic Rydberg energy, μ^* is the reduced exciton mass, which is calculated by $\frac{1}{\mu^*} = \frac{1}{m_e} + \frac{1}{m_h}$, and ε_∞ is the high-frequency dielectric constant.

1.7. Theoretical power conversion efficiency

The power conversion efficiency (PCE) η of a single-junction solar cell is defined as

$$\eta = P_m / P_{in},$$

where P_{in} is the total incident solar energy density (AM 1.5G), and P_m is the maximum output power density, which can be obtained by

$$P_m = I_m V_m = I_{SC} V_{OC} FF,$$

where I_m (V_m) is the maximum current density (voltage), I_{SC} is the short-circuit current density, V_{OC} is the open-circuit voltage, and FF is the fill factor. The current density-voltage relationship, *i.e.* I-V curve can be obtained by [22, 23]

$$I = I_{sc} - I_0 [\exp(eV/K_B T) - 1],$$

here, K_B is the Boltzmann constant, and the short-circuit current density I_{sc} can be obtained by

$$I_{sc} = e \int_0^\infty a(E) I_{sun}(E) dE.$$

The photon absorptivity $a(E)$ is defined as $a(E) = 1 - e^{-2\alpha(E)L}$, where L is the thickness of the absorber layer with a zero-reflectivity front surface and unity-reflectivity back surface, and $\alpha(E)(\alpha(\omega))$ is the optical absorption coefficient calculated by using the first-principles method. $I_{sun}(E)$ is the AM 1.5G standard photon flux at temperature T. The reverse saturation current I_0 is given by

$$I_0 = I_0^r + I_0^{nr} = I_0^r/f_r,$$

where I_0^r and I_0^{nr} are radiative and nonradiative parts, respectively. The fraction of the radiative electron-hole recombination current f_r can be described by

$$f_r = e^{-\Delta/K_B T} = e^{-(E_g^{da} - E_g)/K_B T},$$

here, E_g^{da} is the minimum allowed bandgap and depends on the transition mechanism

of solar absorber. As for the anti-perovskite Ca$_6$CSe$_4$ and Sr$_6$CSe$_4$, they are direct-band-gap compounds with parity-allowed transition between the CBM and VBM, which

means $E_g^{da} = E_g$, then the parameter f_r would be 1. Therefore, the reverse saturation

current I_0 can be calculated by

$$I_0 = I_0^r = e \int_0^\infty a(E) I_{bb}(E,T) dE,$$

here, $I_{bb}(E,T)$ is black-body spectrum at temperature T.

1.8. Concentrator solar cells

In concentrator photovoltaic systems, the concentration ratio X of the solar radiation incident onto the cell represents how many times the solar light is focused and is commonly referred to as 'suns' [24].

At 1sun, the PCE η^{1sun} can be defines as

$$\eta^{1sun} = \frac{I_{SC}^{1sun} V_{OC}^{1sun} FF^{1sun}}{P_{in}^{1sun}},$$

here, P_{in}^{1sun} is the total incident solar energy density (AM 1.5D standard photon flux). V_{OC}^{1sun}, I_{SC}^{1sun}, and FF^{1sun} indicate the short-circuit current density, open-circuit voltage, and fill factor, respectively, and could be gained using the above-mentioned approach.

At X suns, the short-circuit current density can be obtained by $I_{SC}^{Xsuns} = X I_{SC}^{1sun}$. The open-circuit voltage is received by

$$V_{OC}^{Xsuns} = V_{OC}^{1sun} + \frac{k_B T}{e} \ln X,$$

then the fill factor could be calculated from the corresponding open-circuit voltage V_{OC}^{Xsuns} by using the following formula

$$FF^{Xsuns} = \frac{V_{OC}^{Xsuns} - \frac{k_B T}{e} \ln[e V_{OC}^{Xsuns}/k_B T + 0.72]}{V_{OC}^{Xsuns} + \frac{k_B T}{e}}.$$

Given the short-circuit current density, open-circuit voltage, and fill factor, the PCE at X suns can be gained as
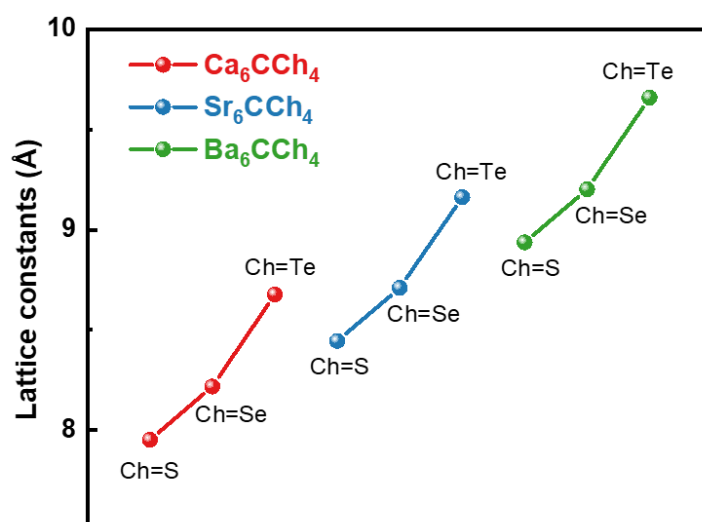
$$\eta^{Xsuns} = \frac{I_{SC}^{Xsuns} V_{OC}^{Xsuns} FF^{Xsuns}}{P_{in}^{Xsuns}} = \eta^{1sun} \left(\frac{FF^{Xsuns}}{FF^{1sun}}\right)\left(1 + \frac{\frac{k_B T}{e}\ln X}{V_{OC}^{1sun}}\right),$$

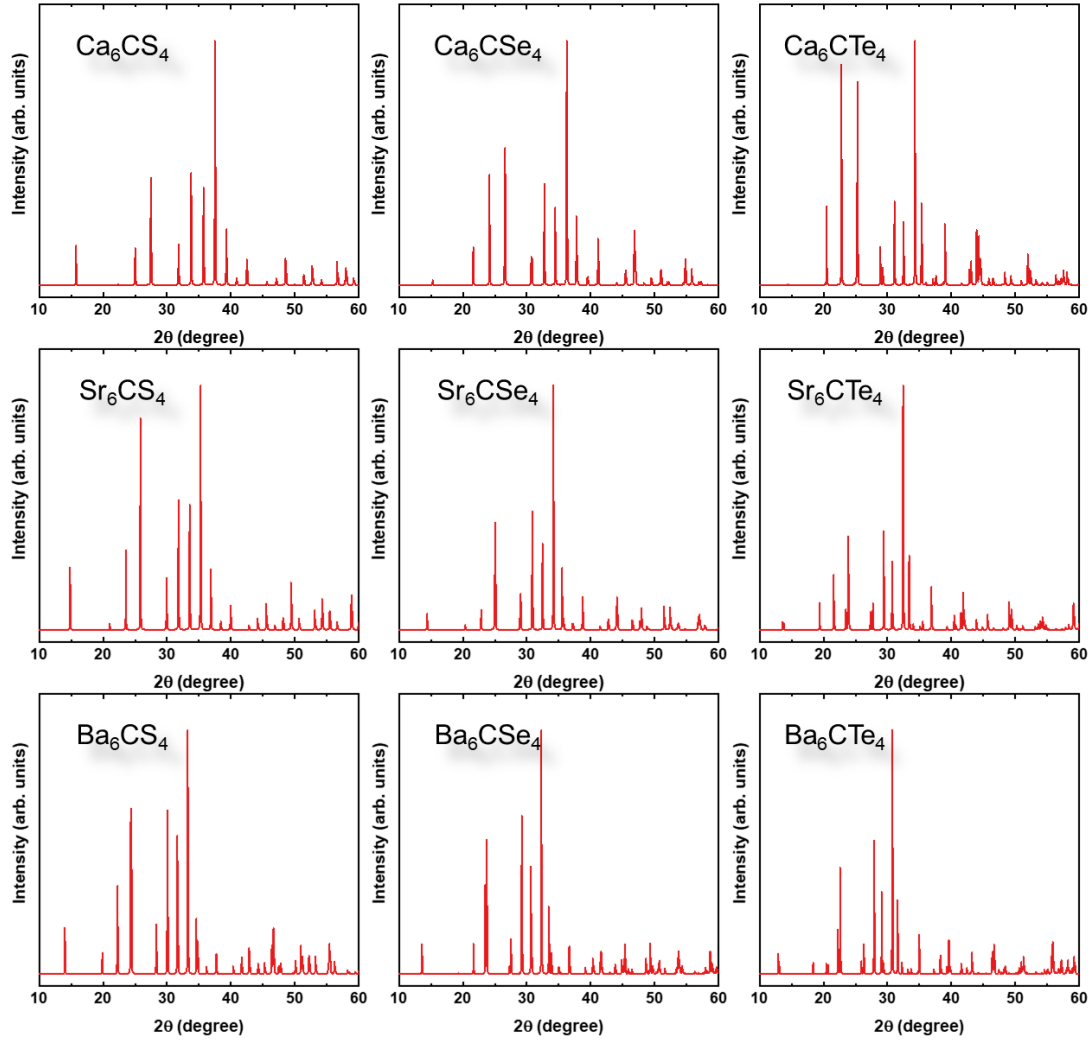here, the total incident solar energy density P_{in}^{Xsuns} is calculated by $P_{in}^{Xsuns} = X P_{in}^{1sun}$

2. Crystal structure and stability
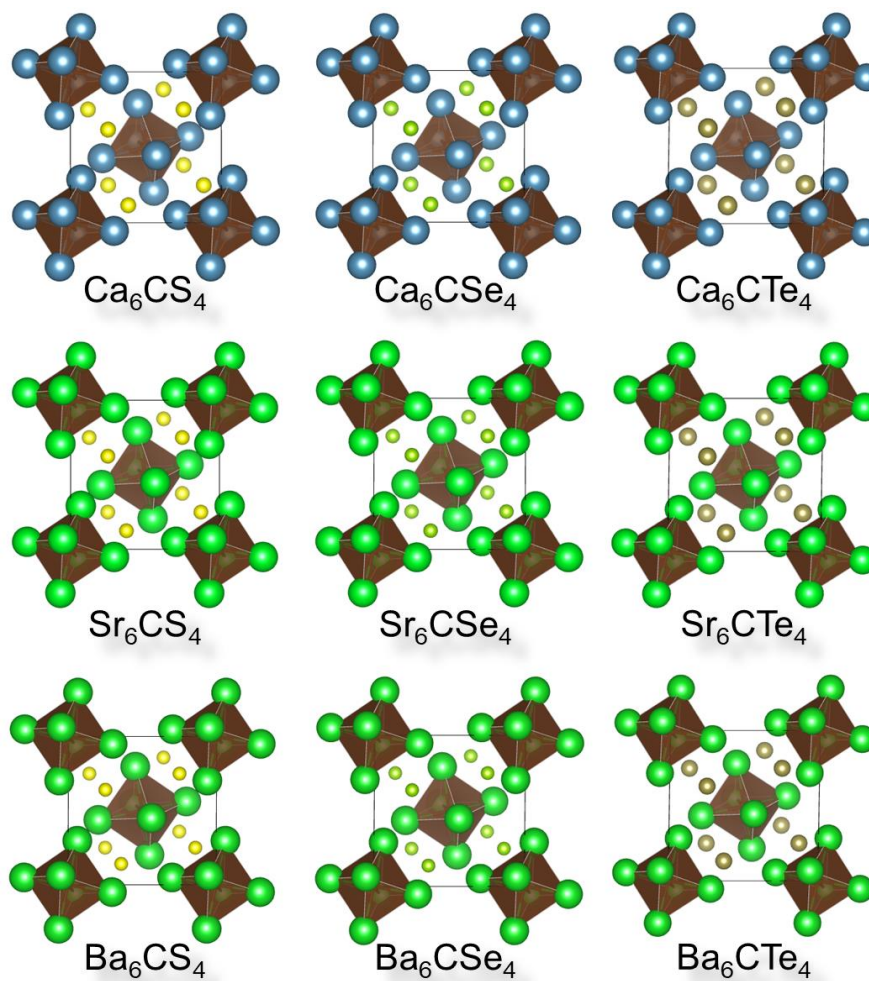
Figure S1 Relaxed rhombohedral lattice of M_6CCh_4 (M=Ca, Sr, Ba; Ch=S, Se, Te) anti-perovskites.

Figure S2 Lattice constants of M_6CCh_4 (M=Ca, Sr, Ba; Ch=S, Se, Te) anti-perovskites.

Figure S3 X-ray diffraction (XRD) spectra of M_6CCh_4 (M=Ca, Sr, Ba; Ch=S, Se, Te) anti-perovskites, in which the angular range and the radiation wavelength are chosen to be 10°-60° and λ=1.54184 (Cu-K_α), respectively.

Table S1 Several possible and stable decomposition compounds of M_6CCh_4 (M=Ca, Sr, Ba; Ch=S, Se, Te) anti-perovskites are listed. Their structural formula and identification number (ID) are collected from the Materials Project [20].

| Formula	ID	Formula	ID	Formula	ID	Formula	ID
Ca	mp-132	Sr	mp-1187073	Ba	mp-122	C	mp-569304
S	mp-96	Se	mp-570481	Te	mp-19	SrC_6	mp-1208630
BaC_6	mp-1214417	CaS	mp-1672	CaSe	mp-1415	CaTe	mp-1519
SrS	mp-1987	SrS_3	mp-1175	SrSe	mp-2758	SrTe	mp-1958
BaS	mp-1500	BaS_2	mp-684	BaS_3	mp-239	BaSe	mp-1253
$BaSe_2$	mp-7547	BaTe	mp-1000				

Table S2 Estimated melting point T_0 [16], decomposition paths and corresponding decomposition energy of M_6CCh_4 (M=Ca, Sr, Ba; Ch=S, Se, Te) anti-perovskites. The decomposition energy is obtained by the difference between the total energy of all decomposition compounds and that of M_6CCh_4. The positive decomposition energy indicates that M_6CCh_4 is stable due to the prohibited decomposition path.

| Compound	T_0 (K)	Decomposition path	Decomposition energy (eV/atom)
Ca_6CS_4	1026	$Ca_6CS_4 \xrightarrow{T \geq T_0} 4CaS+2Ca+C$	-0.20
Ca_6CSe_4	988	$Ca_6CSe_4 \xrightarrow{T \geq T_0} 4CaSe+2Ca+C$	-0.14
Ca_6CTe_4	923	$Ca_6CTe_4 \xrightarrow{T \geq T_0} 4CaTe+2Ca+C$	-0.07
Sr_6CS_4	951	$Sr_6CS_4 \xrightarrow{T \geq T_0} 4SrS+2Sr+C$	-0.27
		$3Sr_6CS_4 \rightarrow 4SrS_3+14Sr+3C$	0.80
		$6Sr_6CS_4 \xrightarrow{T \geq T_0} 24SrS+SrC_6+11Sr$	-0.27
		$6Sr_6CS_4 \rightarrow 8SrS_3+SrC_6+27Sr$	0.79
Sr_6CSe_4	923	$Sr_6CSe_4 \xrightarrow{T \geq T_0} 4SrSe+2Sr+C$	-0.21
		$6Sr_6CSe_4 \xrightarrow{T \geq T_0} 24SrSe+SrC_6+11Sr$	-0.21
Sr_6CTe_4	877	$Sr_6CTe_4 \xrightarrow{T \geq T_0} 4SrTe+2Sr+C$	-0.14
		$6Sr_6CTe_4 \xrightarrow{T \geq T_0} 24SrTe+SrC_6+11Sr$	-0.15
Ba_6CS_4	905	$Ba_6CS_4 \xrightarrow{T \geq T_0} 4BaS+2Ba+C$	-0.24
		$Ba_6CS_4 \rightarrow 2BaS_2+4Ba+C$	0.50
		$3Ba_6CS_4 \rightarrow 4BaS_3+14Ba+3C$	0.76
		$6Ba_6CS_4 \xrightarrow{T \geq T_0} 24BaS+BaC_6+11Ba$	-0.25
		$6Ba_6CS_4 \rightarrow 12BaS_2+BaC_6+23Ba$	0.49
		$6Ba_6CS_4 \rightarrow 8BaS_3+BaC_6+27Ba$	0.75
Ba_6CSe_4	867	$Ba_6CSe_4 \xrightarrow{T \geq T_0} 4BaSe+2Ba+C$	-0.20
		$Ba_6CSe_4 \rightarrow 2BaSe_2+4Ba+C$	0.53
		$6Ba_6CSe_4 \xrightarrow{T \geq T_0} 24BaSe+BaC_6+11Ba$	-0.21
		$6Ba_6CSe_4 \rightarrow 12BaSe_2+BaC_6+23Ba$	0.52
Ba_6CTe_4	830	$Ba_6CTe_4 \xrightarrow{T \geq T_0} 4BaTe+2Ba+C$	-0.15
		$6Ba_6CTe4 \xrightarrow{T \geq T_0} 24BaTe+BaC_6+11Ba$	-0.16
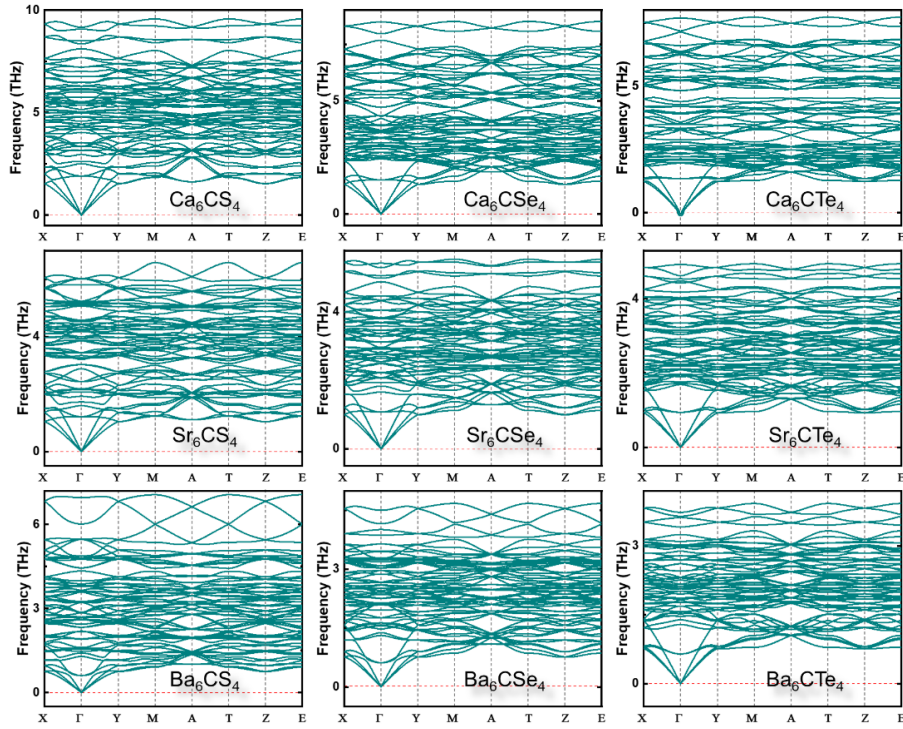
**Figure S4** Phonon spectra of M_6CCh_4 (M=Ca, Sr, Ba; Ch=S, Se, Te) anti-perovskites at room temperature.
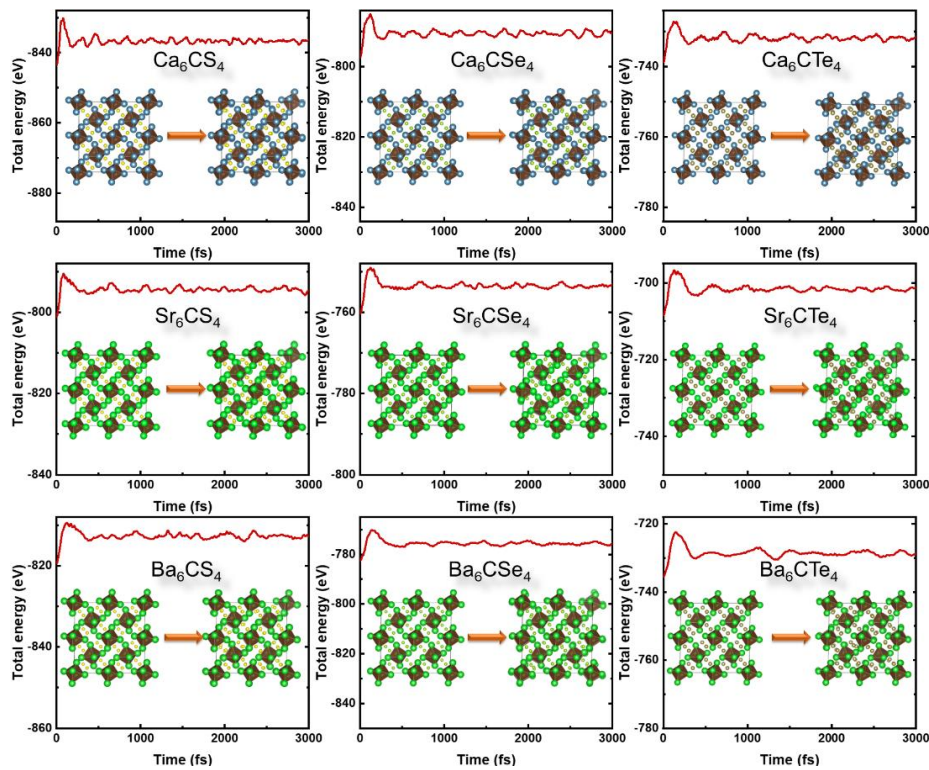
Figure S5 Fluctuation of the total energy of M_6CCh_4 (M=Ca, Sr, Ba; Ch=S, Se, Te) anti-perovskites during the Ab initio molecular dynamics (AIMD) simulation at 300 K within 3000 fs. The inset is the crystal structures before (the left) and after (the right) AIMD.

3. Electronic properties
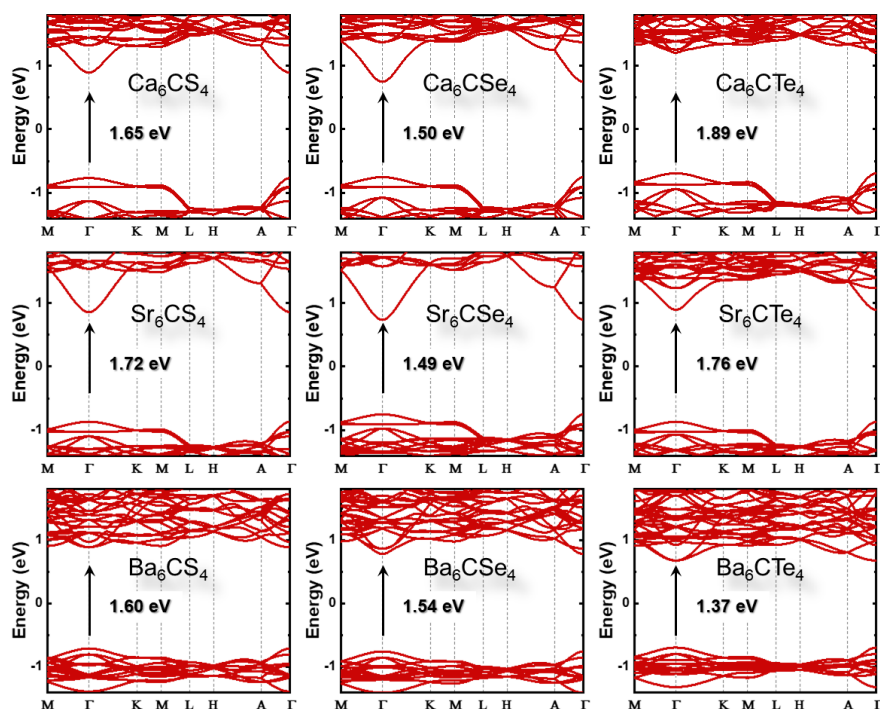
Figure S6 PBE band structures of M_6CCh_4 (M=Ca, Sr, Ba; Ch=S, Se, Te) anti-perovskites, in which the energy gaps are revised by the mBJ potential.
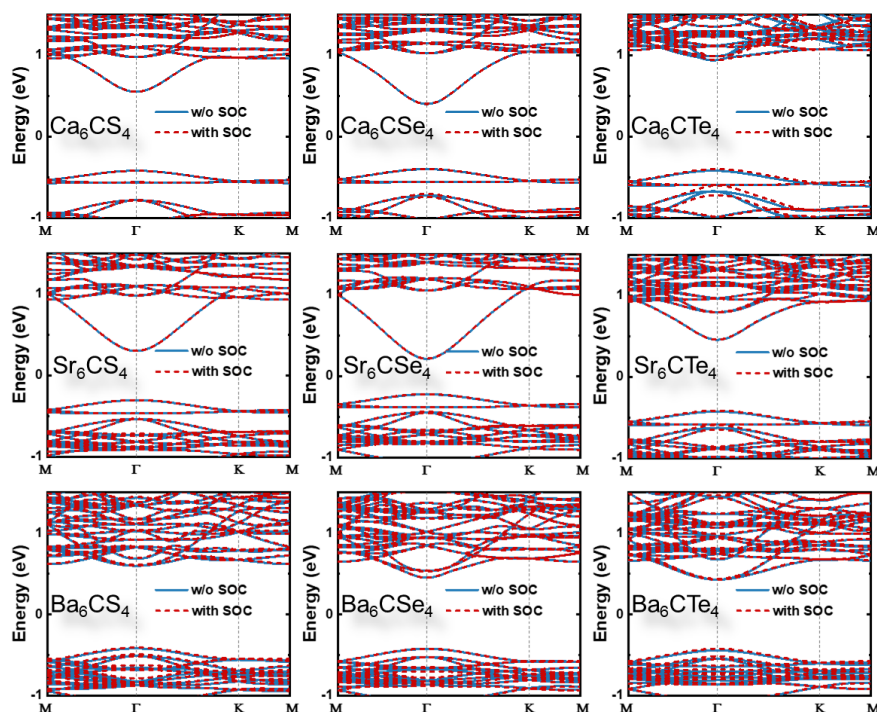

Figure S7 PBE band structures of M_6CCh_4 (M=Ca, Sr, Ba; Ch=S, Se, Te) anti-perovskites without (w/o) (blue solid lines) and with (red dashed lines) spin-orbit coupling (SOC) effect into consideration.

Table S3 Bader net charges in M_6CCh_4 (M=Ca, Sr, Ba; Ch=S, Se, Te) anti-perovskites. The positive (negative) charge value indicates that the corresponding atom loses (gains) electrons.

Compound	Species	Charge	Compound	Species	Charge	Compound	Species	Charge
Ca_6CS_4	Ca	1.372	Ca_6CSe_4	Ca	1.362	Ca_6CTe_4	Ca	1.351
	C	-2.118		C	-2.158		C	-2.196
	S	-1.528		Se	-1.504		Te	-1.477
Sr_6CS_4	Sr	1.364	Sr_6CSe_4	Sr	1.354	Sr_6CTe_4	Sr	1.343
	C	-2.081		C	-2.113		C	-2.143
	S	-1.526		Se	-1.503		Te	-1.479
Ba_6CS_4	Ba	1.282	Ba_6CSe_4	Ba	1.267	Ba_6CTe_4	Ba	1.253
	C	-1.859		C	-1.882		C	-1.911
	S	-1.458		Se	-1.429		Te	-1.403
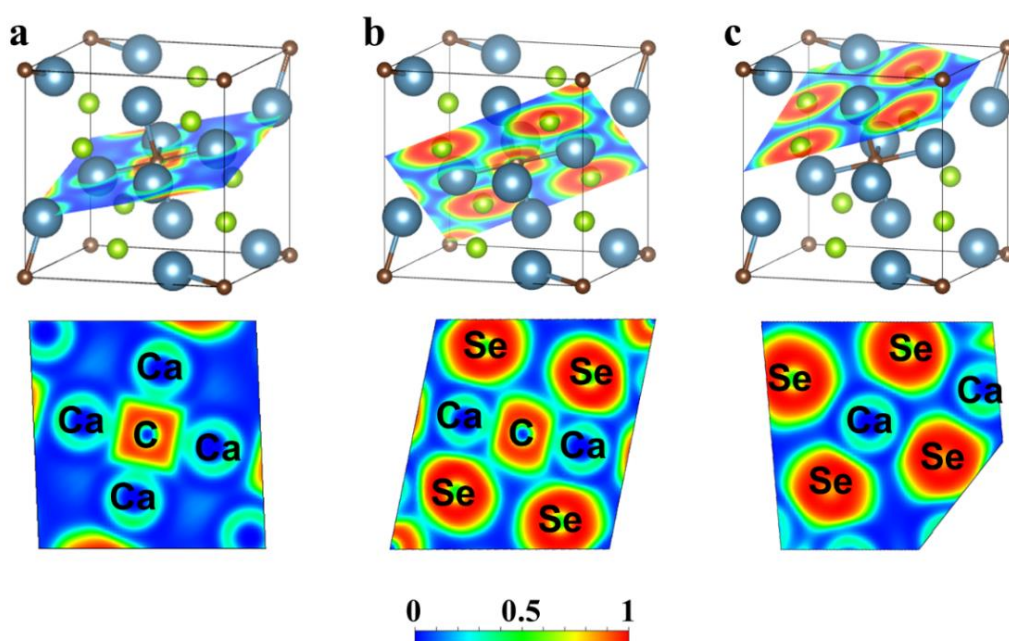
**Figure S8** Electron localization function in Ca_6CSe_4 anti-perovskite.
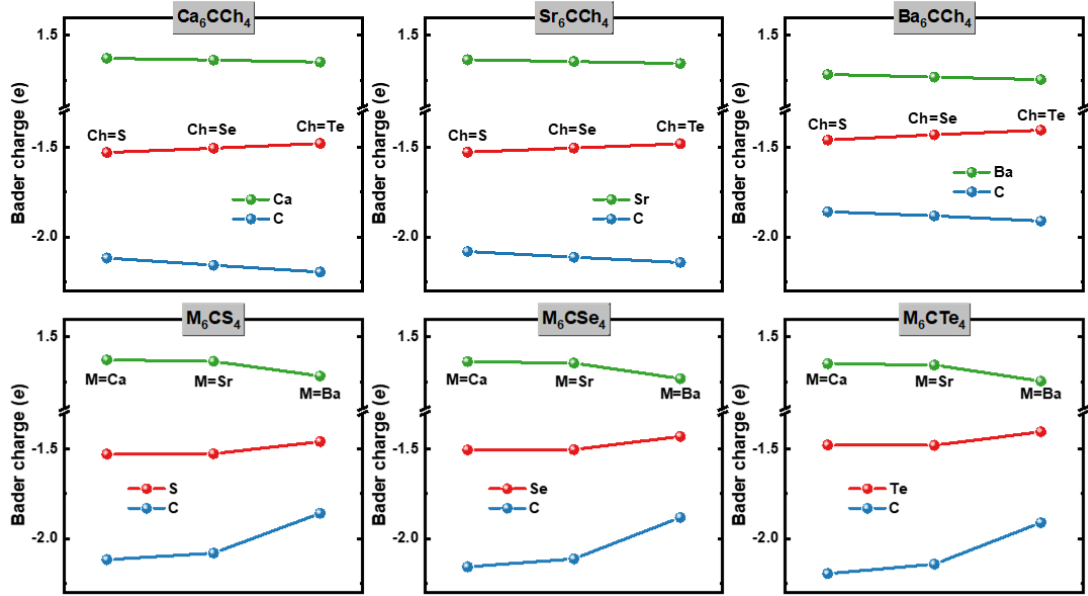
Figure S9 Variation of Bader net charges in M_6CCh_4 (M=Ca, Sr, Ba; Ch=S, Se, Te) anti-perovskites.

Table S4 Quantitative data corresponding to partial charge densities at VBM, CBM, and CB2 (Γ-point) in Ca_6CSe_4 anti-perovskite. The element site is labeled in Figure S10 (b).

Energy level	Element type	Element site	Orbital distribution ratio (%)			
			s	*p*	*d*	Total
VBM	Ca	Ca1-Ca12	0	1	3	4
	C	C1/C2	0	**18**	-	18
	Se	Se1/Se2	0	**6**	0	6
		Se3-Se8	0	1	0	1
CBM	Ca	Ca1-Ca12	**4**	1	1	6
	C	C1/C2	1	0	-	1
	Se	Se1/Se2	**3**	0	0	3
		Se3-Se8	**4**	0	0	4
CB2	Ca	Ca1/Ca5/Ca7/Ca12	0	0	**6**	6
		Ca2/Ca4/Ca8/Ca10	0	0	**8**	8
		Ca3/Ca9	0	0	**9**	9
		Ca6/Ca11	0	0	**10**	10
	C	C1/C2	0	0	-	0
	Se	Se1/Se2/Se5/Se8	0	0	0	0
		Se3/Se4/Se6/Se7	0	0	1	1
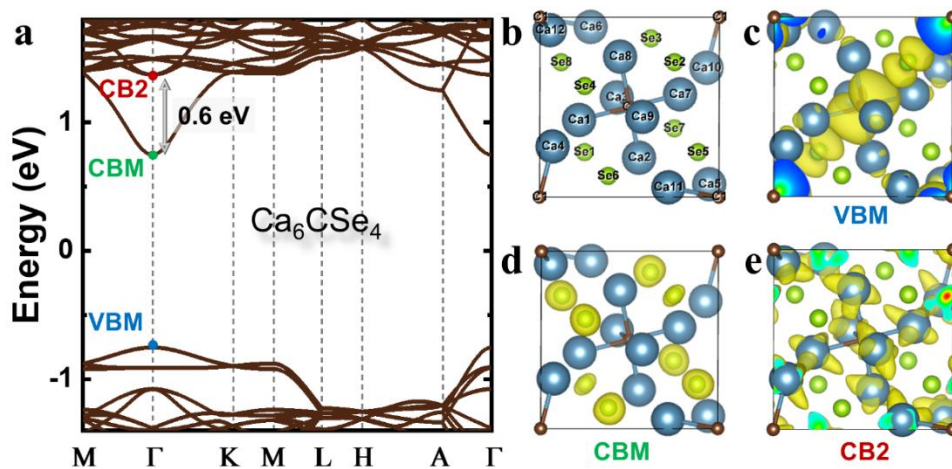
Figure S10 (a) Band structure of Ca_6CSe_4 anti-perovskite, in which the energy positions indicating VBM, CBM, and CB2 are labeled. The energy difference between the CBM and CB2 is 0.6 eV approximately. (b) The crystal structure of Ca_6CSe_4, in which the element sites are marked. The isosurface plot of real space charge distribution at (c) VBM, (d) CBM, and (e) CB2 (Γ-point) in Ca_6CSe_4. The isosurface value is 0.0015 e Å^{-3}.

4. Transport properties

Table S5 Carrier effective mass m^*, ionic screening parameter $1/\varepsilon^*$, electron-phonon coupling constant α, and carrier mobility μ of M_6CCh_4 (M=Ca, Sr, Ba; Ch=S, Se, Te) anti-perovskites along Γ-M, Γ-K, and Γ-A paths, in which e and h indicate electron and hole, respectively.

Compound	$1/\varepsilon^*$	k-path	Carrier					
			e			h		
			m^* (m_0)	α	μ $(cm^2V^{-1}s^{-1})$	m^* (m_0)	α	μ $(cm^2V^{-1}s^{-1})$
MAPbI$_3$	0.17	-	0.104	1.72	197	0.104	1.72	197
Ca$_6$CS$_4$	0.09	Γ-M	0.28	0.88	127	1.95	2.33	5
		Γ-K	0.29	0.90	121	1.97	2.34	5
		Γ-A	0.31	0.93	109	0.24	0.82	163
Ca$_6$CSe$_4$	0.07	Γ-M	0.21	0.74	210	1.63	2.07	8
		Γ-K	0.22	0.76	195	1.67	2.09	7
		Γ-A	0.21	0.74	210	0.20	0.72	226
Ca$_6$CTe$_4$	0.06	Γ-M	0.24	0.70	201	1.30	1.64	14
		Γ-K	0.24	0.70	201	1.34	1.66	13
		Γ-A	0.19	0.63	289	0.20	0.64	264
Sr$_6$CS$_4$	0.08	Γ-M	0.23	0.85	162	1.73	2.34	6
		Γ-K	0.24	0.87	150	1.78	2.37	6
		Γ-A	0.23	0.85	162	0.23	0.85	162
Sr$_6$CSe$_4$	0.07	Γ-M	0.18	0.74	255	1.55	2.17	8
		Γ-K	0.19	0.76	232	1.58	2.20	8
		Γ-A	0.16	0.70	306	0.17	0.72	279
Sr$_6$CTe$_4$	0.06	Γ-M	0.20	0.76	238	1.29	1.92	12
		Γ-K	0.21	0.78	220	1.29	1.92	12
		Γ-A	0.18	0.72	279	1.29	1.92	12
Ba$_6$CS$_4$	0.08	Γ-M	0.70	1.58	26	1.13	2.01	12
		Γ-K	0.83	1.73	19	1.17	2.05	11
		Γ-A	0.86	1.76	18	0.36	1.14	76
Ba$_6$CSe$_4$	0.07	Γ-M	0.24	0.98	148	1.13	2.14	12
		Γ-K	0.27	1.04	122	1.16	2.16	11
		Γ-A	0.24	0.98	148	0.28	1.06	116
Ba$_6$CTe$_4$	0.07	Γ-M	0.45	1.30	61	0.98	1.92	17
		Γ-K	0.50	1.37	51	0.99	1.93	17
		Γ-A	0.86	1.80	21	0.25	0.97	154

Table S6 Electronic (high-frequency) ε_{elec}, ionic ε_{ion}, and static ε_0 dielectric constants of M_6CCh_4 (M=Ca, Sr, Ba; Ch=S, Se, Te) anti-perovskites.

Compound	ε_{elec}	ε_{ion}	ε_0
$MAPbI_3$	5.0	28.5	33.50
Ca_6CS_4	7.43	12.7	20.13
Ca_6CSe_4	7.90	11	18.90
Ca_6CTe_4	8.48	8.8	17.28
Sr_6CS_4	7.76	14.59	22.35
Sr_6CSe_4	8.26	11.91	20.17
Sr_6CTe_4	8.35	9.15	17.50
Ba_6CS_4	8.64	21.12	29.76
Ba_6CSe_4	8.86	16.71	25.57
Ba_6CTe_4	9.04	12.94	21.98
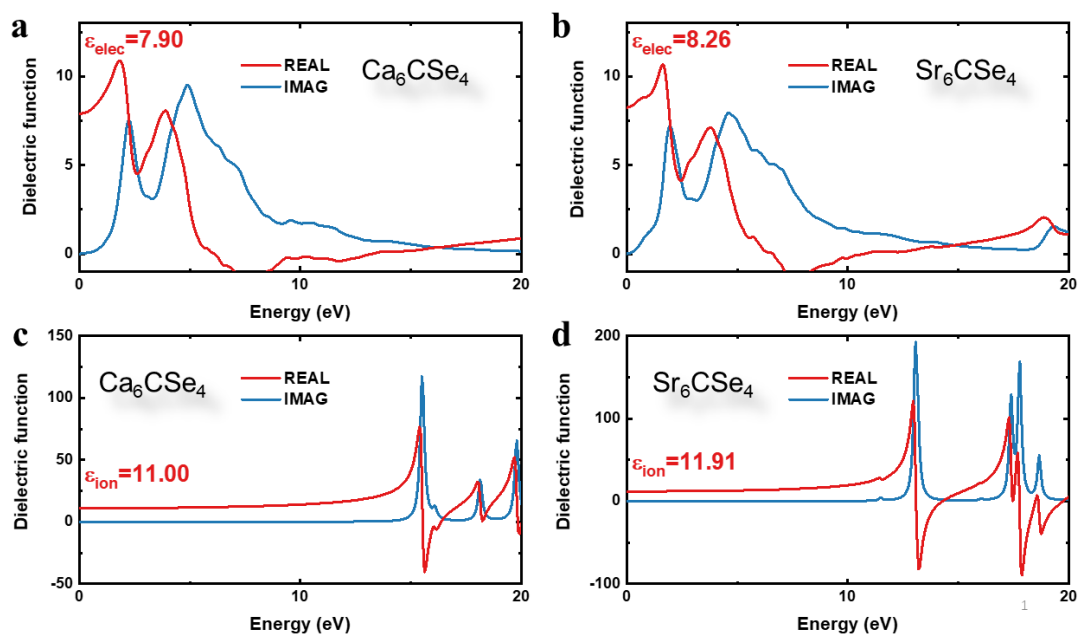
Figure S11 Dielectric properties of (a, c) Ca_6CSe_4 and (b, d) Sr_6CSe_4 anti-perovskites. The calculated (a, b) electronic and (c, d) ionic contributions to the real and imaginary part of the dielectric function. The static dielectric constant ε_0 is calculated by $\varepsilon_0 = \varepsilon_{elec} + \varepsilon_{ion}$.

5. Optical properties
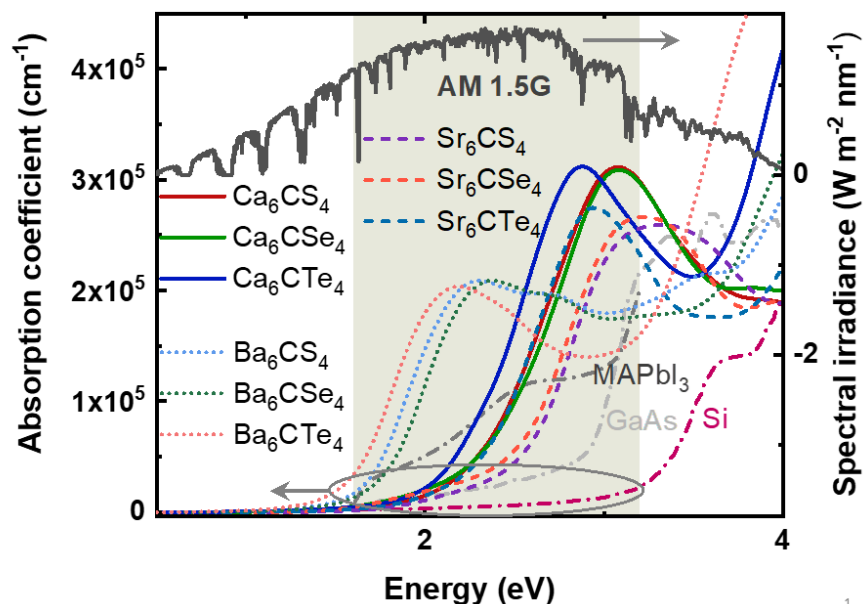
Figure S12 Optical absorption coefficient of M_6CCh_4 (M=Ca, Sr, Ba; Ch=S, Se, Te) anti-perovskites and those of photovoltaic compounds including Si, GaAs, and MAPbI₃. The inset is the AM 1.5G spectrum. The dash area indicates the visible-light region.

Table S7 Exciton binding energy E_b of M_6CCh_4 (M=Ca, Sr, Ba; Ch=S, Se, Te) anti-perovskites. The reduced exciton mass μ^* and high-frequency dielectric constant ε_∞ are also listed.

Compound	ε_∞	μ^* (m_0)	E_b (meV)
Ca_6CS_4	7.43	0.24	59
Ca_6CSe_4	7.90	0.18	39
Ca_6CTe_4	8.48	0.18	34
Sr_6CS_4	7.76	0.20	44
Sr_6CSe_4	8.26	0.15	30
Sr_6CTe_4	8.35	0.16	31
Ba_6CS_4	8.64	0.42	76
Ba_6CSe_4	8.86	0.19	34
Ba_6CTe_4	9.04	0.33	55

6. Theoretical power conversion efficiency
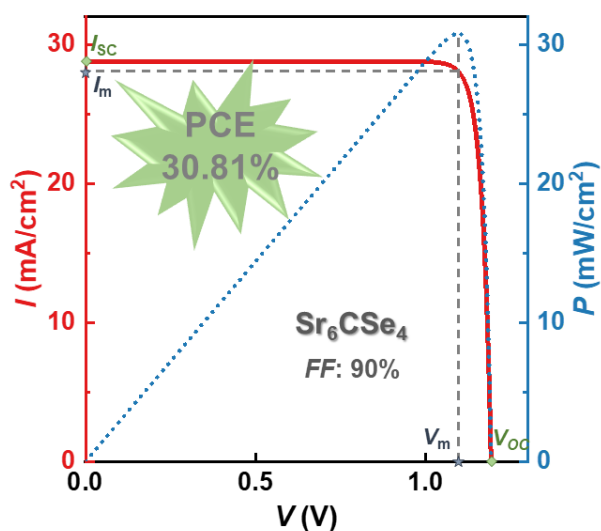
Figure S13 *I-V* and *P-V* curves of the 3 μm-thick Sr₆CSe₄ anti-perovskite, and the corresponding parameters, such as the short-circuit current density I_{SC}, open-circuit voltage V_{OC}, maximum current density (voltage) I_m (V_m), and fill factor *FF* are also given.

Table S8 Calculated maximum current density I_m (voltage V_m), short-circuit current density I_{SC}, open-circuit voltage V_{OC}, maximum output power density P_m, fill factor FF, and PCE of Ca₆CSe₄ and Sr₆CSe₄ anti-perovskites.

Compound	Thickness (μm)	I_m (mA/cm²)	V_m (V)	I_{SC} (mA/cm²)	V_{OC} (V)	P_m (mW/cm²)	FF (%)	PCE (%)
Ca₆CSe₄	3	27.55	1.12	28.19	1.22	30.83	89	30.83
Sr₆CSe₄	3	28.13	1.10	28.79	1.20	30.81	90	30.81
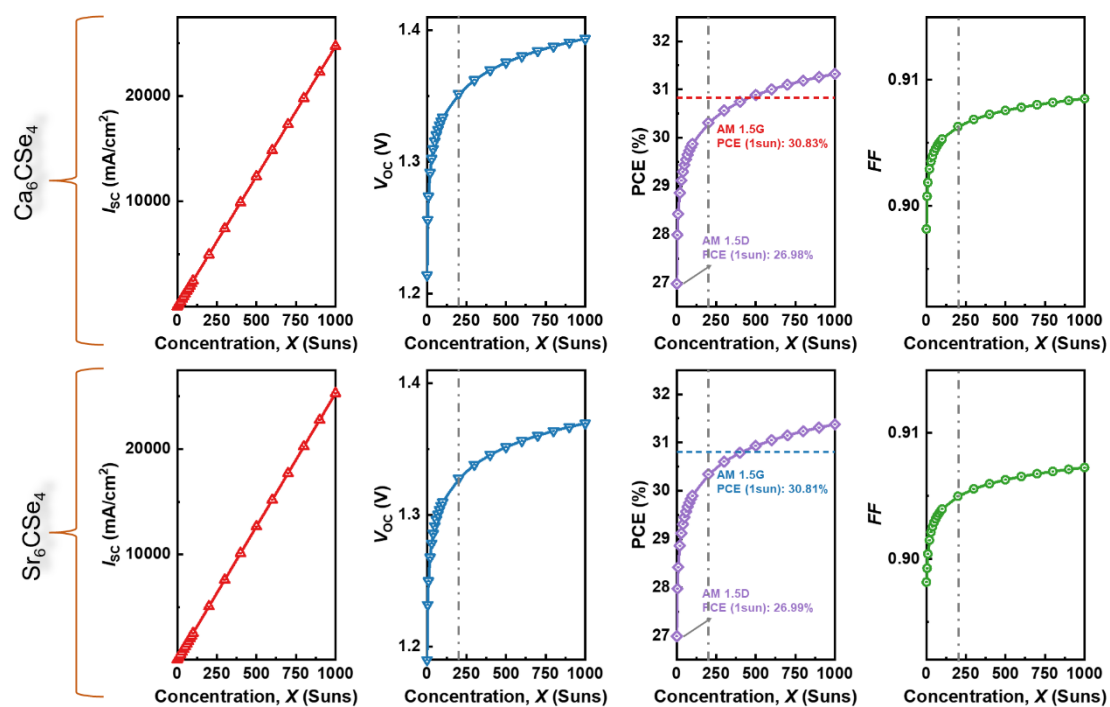
Figure S14 Several vital parameters including the short-circuit current density I_{SC}, open-circuit voltage V_{OC}, PCE, and fill factor FF versus the concentration ratio X in 3 μm-thick Ca_6CSe_4 and Sr_6CSe_4 anti-perovskites. The red and blue dashed lines indicate the PCE values of the 3 μm-thick Ca_6CSe_4 and Sr_6CSe_4 under AM 1.5G spectral radiation, respectively.

References

[1] G. Kresse and J. Hafner, *Phys. Rev. B*, 1993, 47, 558-561.

[2] J. P. Perdew, K. Burke and M. Ernzerhof, *Phys. Rev. Lett.*, 1996, 77, 3865-3868.

[3] P. E. Blöchl, *Phys. Rev. B*, 1994, 50, 17953-17979.

[4] G. Kresse and D. Joubert, *Phys. Rev. B*, 1999, 59, 1758-1775.

[5] F. Tran and P. Blaha, *Phys. Rev. Lett.*, 2009, 102, 226401.

[6] A. D. Becke and M. R. Roussel, *Phys. Rev. A*, 1989, 39, 3761–3767.

[7] R. P. Feynman, *Phys. Rev.*, 1955, 97, 660-665.

[8] R. P. Feynman, R. W. Hellwarth, C. K. Iddings and P. M. Platzman, *Phys. Rev.*, 1962, 127, 1004-1017.

[9] M. Sendner, P. K. Nayak, D. A. Egger, S. Beck, C. Müller, B. Epding, W. Kowalsky, L. Kronik and H. J. Snaith, A. Pucci and R. Lovrinčić, *Mater. Horiz.*, 2016, 3, 613-620.

[10] I. Biaggio, R. W. Hellwarth and J. P. Partanen, *Phys. Rev. Lett.*, 1997, 78, 891-894.

[11] R. W. Hellwarth and I. Biaggio, *Phys. Rev. B*, 1999, 60, 299-307.

[12] J. M. Frost, *Phys. Rev. B*, 2017, 96, 195202.

[13] M. Gajdoš, K. Hummer, G. Kresse, J. Furthmüller and F. Bechstedt, *Phys. Rev. B*, 2006, 73, 045112.

[14] A. Moscowitz, *Adv. Chem. Phys.*, 1962, 4, 67-112.

[15] S. Saha, T. P. Sinha and A. Mookerjee, *Phys. Rev. B*, 2000, 62, 8828-8834.

[16] I. Johnston, G. Keeler, R. Rollins and S. Spicklemire, Solid State Physics Simulations. The Consortium for Upper Level Physics Software, Wiley, New York, 1996.

[17] W. Voigt, *Ann. Phys.*, 1889, 38, 573.

[18] A. Reuss and Z. Angew. *Math. Mech.*, 1929, 9, 49.

[19] R. Hill, *Proc. Phys. Soc. A*, 1952, 65, 349.

[20] V. Wang, N. Xu, J. C. Liu, G. Tang and W. T. Geng, *Computer Physics Communications*, 2021, *267*, 108033.

[21] X.-G. Zhao, J.-H. Yang, Y. Fu, D. Yang, Q. Xu, L. Yu, S.-H. Wei and L. Zhang, *J. Am. Chem. Soc.*, 2017, 139, 2630–2638.

[22] L. Yu and A. Zunger, *Phys. Rev. Lett.*, 2012, 108, 068701.

[23] L. Yu, R. S. Kokenyesi, D. A. Keszler and A. Zunger, *Adv. Energy Mater.*, 2013, 3, 43-48.

[24] A. Luque and S. Hegedus, Handbook of Photovoltaic Science and Engineering; John Wiley & Sons, 2011.